LETTER

doi:10.1038/nature14122

EZH2 inhibition sensitizes *BRG1* and *EGFR* mutant lung tumours to TopoII inhibitors

Christine M. Fillmore[1,2,3], Chunxiao Xu[4,5], Pooja T. Desai[1], Joanne M. Berry[1], Samuel P. Rowbotham[1,2,3], Yi-Jang Lin[2], Haikuo Zhang[4,5], Victor E. Marquez[6], Peter S. Hammerman[4], Kwok-Kin Wong[4,5] & Carla F. Kim[1,2,3]

Non-small-cell lung cancer is the leading cause of cancer-related death worldwide[1]. Chemotherapies such as the topoisomerase II (TopoII) inhibitor etoposide effectively reduce disease in a minority of patients with this cancer[2,3]; therefore, alternative drug targets, including epigenetic enzymes, are under consideration for therapeutic intervention[4]. A promising potential epigenetic target is the methyltransferase EZH2, which in the context of the polycomb repressive complex 2 (PRC2) is well known to tri-methylate histone H3 at lysine 27 (H3K27me3) and elicit gene silencing[5]. Here we demonstrate that EZH2 inhibition has differential effects on the TopoII inhibitor response of non-small-cell lung cancers *in vitro* and *in vivo*. *EGFR* and *BRG1* mutations are genetic biomarkers that predict enhanced sensitivity to TopoII inhibitor in response to EZH2 inhibition. *BRG1* loss-of-function mutant tumours respond to EZH2 inhibition with increased S phase, anaphase bridging, apoptosis and TopoII inhibitor sensitivity. Conversely, *EGFR* and *BRG1* wild-type tumours upregulate *BRG1* in response to EZH2 inhibition and ultimately become more resistant to TopoII inhibitor. *EGFR* gain-of-function mutant tumours are also sensitive to dual EZH2 inhibition and TopoII inhibitor, because of genetic antagonism between *EGFR* and BRG1. These findings suggest an opportunity for precision medicine in the genetically complex disease of non-small-cell lung cancer.

To validate that EZH2 is an important target for non-small-cell lung cancer (NSCLC), we generated a 116-gene lung cancer *EZH2* co-expression gene signature (Supplementary Table 1). This signature had predictive power for cancer progression using the Director's Challenge data set of 416 human lung adenocarcinomas[6], partly because of stratification of later-stage tumours to the *EZH2* high group (Extended Data Fig. 1a). To control for this covariate, exclusively stage 1 and moderately differentiated tumours were examined, confirming that the signature could robustly further stratify patients into risk groups (Fig. 1a). Gene ontology analysis revealed that the *EZH2* co-expression signature was highly enriched for cell cycle, DNA synthesis and DNA repair genes (Supplementary Table 2). One of the genes highly co-expressed with *EZH2* in primary tumours was topoisomerase 2A (*TOP2A*), which encodes the TopoII helicase targeted by etoposide.

To test EZH2 inhibition as a therapy for NSCLC, *EZH2* expression was stably knocked down with one of two different small hairpins in a panel of NSCLC cell lines. Western blot confirmed that EZH2 protein and catalytic mark, H3K27me3, were decreased in each transduced cell line and could be rescued by *EZH2* expression from a second lentivirus (Fig. 1b and Extended Data Fig. 1b). We then determined etoposide half-maximum inhibitory concentration (IC_{50}) at 4 days. Of the seven lines, HCC15, A549, H157 and PC9, termed 'sensitized' lines, had lower etoposide IC_{50} when *EZH2* was knocked down. Conversely, H460, H23 and Sw1573 cell lines, termed 'protected' lines, had higher etoposide IC_{50} as shEZH2 lines (Fig. 1c). Rescue of EZH2 levels completely abrogated the change in etoposide IC_{50} driven by the 3′ untranslated region (UTR) targeting hairpin (A549 and Sw1573; Fig. 1c, grey bars). The sensitized and protected phenotypes were not due to differential degrees of *EZH2* knockdown (Extended Data Fig. 1b, c).

Next, we used pharmacological EZH2 inhibition via the *S*-adenosylhomocystein hydrolase inhibitor, DZNep, which causes proteosomal degradation of PRC2 components including EZH2 (refs 7, 8) and the specific EZH2 methyltransferase inhibitor, GSK126 (ref. 9). Western blot confirmed that 4 days of 1 μM DZNep effectively reduced EZH2 protein and H3K27me3, and 10 μM GSK126 for 4 days or 2 μM GSK126 for 9 days caused a decrease in H3K27me3 levels yet EZH2 remained unchanged (Fig. 1d and Extended Data Fig. 2a). Fourteen of 26 NSCLC cell lines were more sensitive to 4-day etoposide in the presence of 1 μM DZNep, while the other lines were less sensitive to the chemotherapy in the presence of DZNep (Fig. 1e and Extended Data Fig. 2b). For the sensitized lines, pretreatment with 2 μM GSK126 for 9 days sensitized the lines to 4-day etoposide with continued GSK126 treatment (14 days total). For the protected lines, 10 μM of GSK126 for 4 days best recapitulated the etoposide protection caused by DZNep and shEZH2 (Fig. 1e and Extended Data Fig. 2c). IC_{50} shift results were validated with the Chou–Talalay combination index[10], demonstrating strong synergism (combination index < 0.48) between DZNep and etoposide as well as synergism (combination index < 0.64) between GSK126 and etoposide (Fig. 1f and Supplementary Table 3). The combination index assay also confirmed drug antagonism (combination index > 1) in the protected lines.

We examined the mutational annotation available for the NSCLC lines and found that 12 of 14 sensitized cell lines harboured inactivating mutations in *BRG1* (*SMARCA4*) or activating mutations in *EGFR*, while 10 of 12 protected cell lines were wild type (WT) for the two genes (Supplementary Table 4 and Extended Data Fig. 2c; Fisher's exact test, $P = 0.001$). Cell lines segregated into the same genotype-specific protected and sensitized classes when a different TopoII inhibitor, doxorubicin[11], was combined with DZNep (Extended Data Fig. 2d).

To determine whether the protected and sensitized phenotypes could be observed *in vivo*, we treated xenograft-bearing mice with etoposide and EZH2 inhibition (EZH2i). For the sensitized *BRG1* mutant cell line H157, early treatment with dual etoposide and DZNep therapy prevented tumours from forming in four out of six mice, proving more efficacious than etoposide or DZNep alone (Fig. 2a and Extended Data Fig. 3a, b). In contrast, the protected H23 xenografts that received early dual therapy grew significantly larger than those treated with either DZNep or etoposide alone (Fig. 2b and Extended Data Fig. 3b). Furthermore, in mice with established *EGFR*-driven PC9 xenografts, the combination of GSK126 and etoposide prevented tumour growth (Fig. 2c).

Next, mouse models of lung cancer predicted to be sensitized ($EGFR^{T790M;L858R}$ transgenic; *EGFR* hereafter[12]) or protected ($Kras^{G12D/+}$; $p53^{\Delta/\Delta}$; *Kras*/*p53* hereafter[13]) tumour types were treated with DZNep and etoposide. The *Kras*/*p53* model, WT for *Brg1* and *Egfr*, represents a predicted 'protected' cancer, whereas the *EGFR* model, driven by oncogenic *EGFR*, represents a predicted 'sensitized' cancer. Etoposide,

[1]Stem Cell Program, Boston Children's Hospital, Boston, Massachusetts 02115, USA. [2]Department of Genetics, Harvard Medical School, Boston, Massachusetts 02115, USA. [3]Harvard Stem Cell Institute, Cambridge, Massachusetts 02138, USA. [4]Department of Medical Oncology, Dana-Farber Cancer Institute, Boston, Massachusetts 02115, USA. [5]Belfer Institute for Applied Cancer Science, Dana-Farber Cancer Institute, Boston, Massachusetts 02115, USA. [6]Chemical Biology Laboratory, National Cancer Institute, National Institutes of Health, Frederick, Maryland 21702, USA.

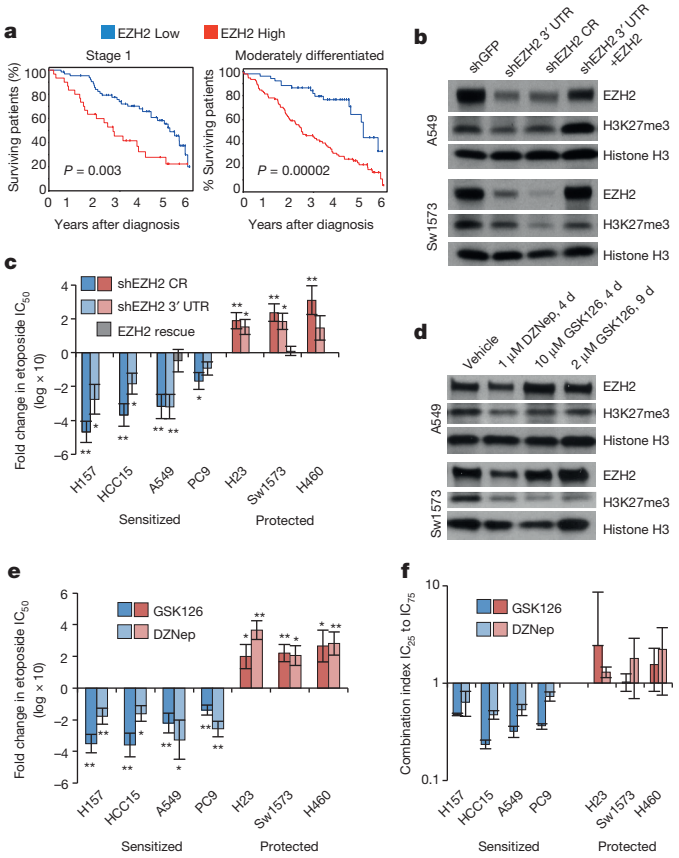

Figure 1 | EZH2i sensitizes BRG1 or EGFR mutants to TopoIIi. a, Director's Challenge samples were hierarchically clustered into two risk groups using the *EZH2* co-expression signature (Supplementary Table 1). The Kaplan–Meier curves only for stage 1 ($n = 94$) or only for moderately differentiated tumours ($n = 142$) to 6 years after diagnosis are shown. **b**, Western blot for EZH2 and H3K27me3 on indicated transduced lines; total histone H3 is shown as loading control. CR indicates a coding region targeting hairpin. **c**, Fold change ± s.e.m. in etoposide IC_{50} between transduced lines ($n = 3$ biological replicates for HCC15, A549, PC9, H23 and Sw1573, $n = 4$ biological replicates for HCC15 and H460, rescues $n = 3$ biological replicates; $^*P < 0.04$, $^{**}P < 0.01$). **d**, Western blot for EZH2 and H3K27me3 on lines treated with indicated drugs. **e**, Fold change ± s.e.m. in etoposide IC_{50} between vehicle-treated and drug-treated lines ($n = 3$ biological replicates for all except $n = 4$ biological replicates for H157 + DZNep; $^*P < 0.04$, $^{**}P < 0.01$). **f**, Average Chou–Talalay combination index values ± s.e.m. (also see Supplementary Table 3) for fractions affected equivalent to IC_{25}–IC_{75} ($n = 3$ biological replicates).

DZNep, or combination therapy was then administered to randomized cohorts of mice with radiographically documented lung masses for 4 weeks (Fig. 2d). Marked tumour regression in the *EGFR* model was observed in response to 4 weeks of dual etoposide and DZNep treatment, while mice in the other treatment arms showed continued tumour growth (Fig. 2e and Extended Data Fig. 4a). In striking contrast, the *Kras*/*p53* tumours proceeded to grow despite dual treatment (Fig. 2f). DZNep efficacy was confirmed by EZH2 immunohistochemistry for both models (Extended Data Fig. 4b, c).

To address the mechanism through which EZH2i changed sensitivity to TopoII inhibitor (TopoIIi), we considered the physical interaction between BRG1 and TopoII that allows for increased TopoII function[14]. Because BRG1 and EZH2 are known to be genetically antagonistic[15], we hypothesized that protected cell lines upregulated *BRG1* in response to EZH2i and thereby had increased TopoII function. *BRG1* transcript measured by quantitative PCR with reverse transcription (RT-qPCR) was reproducibly increased by DZNep treatment, although *BRG1* levels were not significantly different when the cells were treated with GSK126 (Fig. 3a). To assess the function of BRG1-containing BAF complexes we quantified anaphase bridges, which are known to indicate a failure of TopoII to decatenate DNA before mitosis and can be attributable to BAF complex dysfunction (Extended Data Fig. 5a). DZNep or GSK126 treatment increased anaphase bridges in *BRG1* mutant cell lines and decreased anaphase bridges in WT cells (Fig. 3b and Extended Data Fig. 5b). *EGFR* mutant cells, despite BRG1 upregulation, also had increased anaphase bridging with DZNep or GSK126 treatment and showed high levels of EGFR in dividing cells (Extended Data Fig. 5c).

We next examined cell cycle and apoptosis dynamics of the lines. While the protected lines showed no difference in apoptotic levels in etoposide compared with dual-treated cultures, the sensitized lines had significantly higher apoptotic fractions in dual-treated cultures than in cultures treated with etoposide as a single agent (Fig. 3c). Furthermore, protected etoposide-treated lines had an average of 13.5% fewer cells in

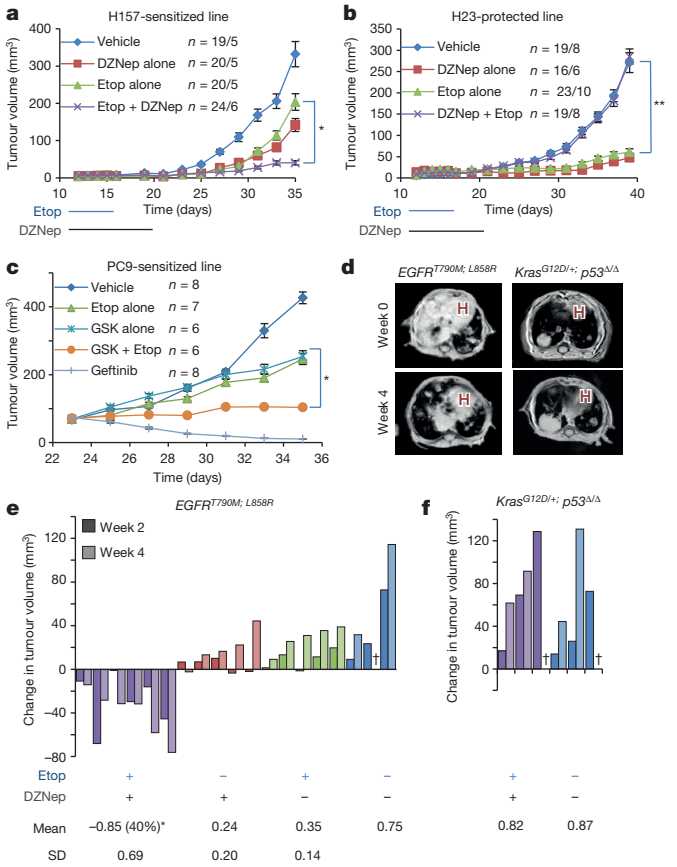

Figure 2 | *In vitro* sensitivities to EZH2i plus TopoIIi predict *in vivo* responses. Either the H157 (**a**) or the H23 (**b**) cell line was injected into the flanks of Nude mice and tumours were allowed to form. On day 12, mice were randomly segregated into cohorts that received either placebo, DZNep, etoposide or dual therapy for 2 weeks, and average tumour size ± s.e.m. were plotted (n for tumours/mice in each arm indicated on graphs; $^*P = 0.002$, $^{**}P = 0.0005$ dual versus etoposide). **c**, The PC9 cell line was injected into the flanks of Nude mice and tumours were allowed to grow to 70 mm^3. Mice were then treated with etoposide, GSK126, dual therapy or gefitinib (as a positive control) for 2 weeks, and average tumour size ± s.e.m. were plotted (n indicated on legend, mice with one tumour each; $P < 0.008$ for dual versus etoposide or GSK126 alone). **d**, Representative magnetic resonance images of mice of indicated genotypes on combination etoposide plus DZNep treatment at 0 and 4 weeks after treatment initiation. H, heart area. **e**, Waterfall plot depicting tumour growth ± s.e.m. of $EGFR^{T790M;L858R}$ tumours after 2 weeks and 4 weeks of treatment with vehicle (blue), etoposide (green), DZNep (red) and etoposide plus DZNep (purple). The y axis indicates percentage tumour growth versus day 0. Each bar represents an individual mouse (†the mouse died before the magnetic resonance imaging time point). Statistical analyses were performed on the 4-week $\log_2$-transformed data ($P = 0.008$ dual versus DZNep and $P = 0.004$ dual versus etoposide). **f**, Waterfall plot depicting tumour growth ± s.e.m. of $Kras^{G12D/+};p53^{\Delta/\Delta}$ tumours after 2 weeks and 4 weeks of treatment with vehicle (blue) and etoposide plus DZNep (purple).

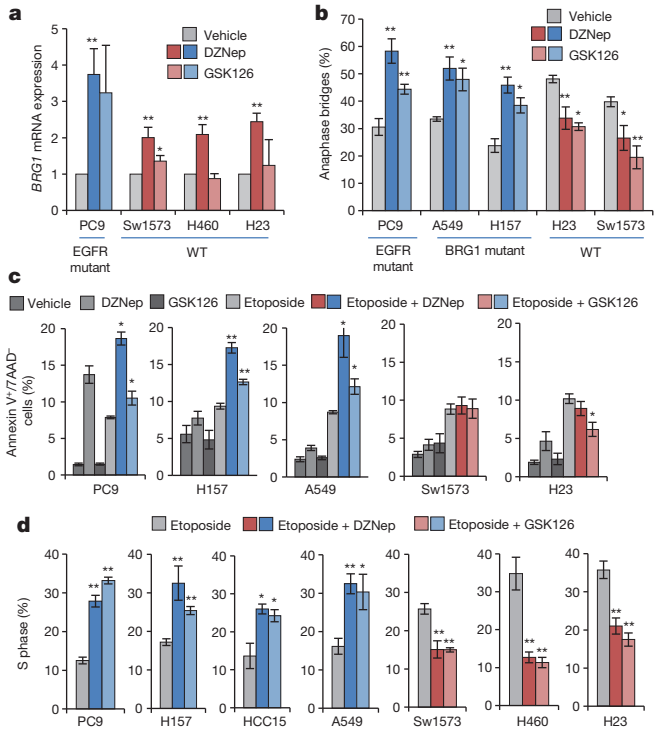

Figure 3 | Dual EZH2i and TopoIIi differentially affects cell cycle, apoptosis and anaphase bridging. **a**, RT-qPCR for average expression of *BRG1* ± s.e.m. in indicated cell lines in response to 4 days of 1 μM DZNep or 10 μM GSK126 ($n = 6$ biological replicates for DZNep, $n = 3$ biological replicates for GSK126; $^*P < 0.05$, $^{**}P < 0.008$). **b**, Average percentage of anaphase structures with bridges ± s.e.m. in vehicle-, DZNep- or GSK126-treated cell lines ($n \geq 3$ biological replicates and indicated in Methods; $^*P < 0.04$, $^{**}P < 0.02$). **c**, Average percentage annexin $V^+/7AAD^-$ cells ± s.e.m. quantified by flow cytometry on cell lines cultured with indicated treatments for 3 days ($n = 4$ biological replicates; $^*P < 0.03$, $^{**}P < 0.001$ for etoposide versus dual-treated or DZNep versus dual treatment for PC9). **d**, 7AAD cell cycle flow cytometry was performed on cell lines with or without 5 μM etoposide or 1 μM DZNep for 4 days. The average percentage S phase ± s.e.m. of each culture is plotted ($n = 3$ biological replicates for HCC15, A549, PC9 and H23, $n = 4$ biological replicates for H157 and Sw1573; $^*P < 0.05$ $^{**}P < 0.009$).

S phase in response to DZNep or shEZH2 compared with treatment with etoposide alone, suggesting these lines undergo cell cycle arrest sparing them from apoptosis. In contrast, sensitized etoposide-treated lines had an average of 16.5% more cells in S phase in response to DZNep or shEZH2 (Fig. 3d and Extended Data Fig. 6a), suggesting that apoptosis of G2/M cells that could not repair anaphase bridges contributed to enrichment for S phase.

While the links between EZH2, BRG1 and TopoII explained increased sensitivity of *BRG1* mutants to TopoIIi, it was still unclear why *EGFR* mutants behaved similarly. In our panel of cell lines, 30% had a *BRG1* mutation and 23% had an *EGFR* mutation; however, none had both *BRG1* and *EGFR* mutations (Supplementary Table 4 and Extended Data Fig. 7a; Fisher's exact test $P = 0.005$). Similarly, in a panel of 412 sequenced primary adenocarcinomas[16,17], 65 (15.7%) had mutation in *EGFR*, while 33 (8%) had mutations in *BRG1*. With these allele frequencies, 1.25% of the tumour samples were expected to have both *BRG1* and *EGFR* mutations; however, only 1 (0.2%) was observed (Fisher's exact test, $P = 0.019$, EGFR R574L). The negative correlation of *BRG1* and *EGFR* mutations suggests that they may be functionally redundant—BRG1 loss may be permissive for high EGFR expression. Supporting this idea, a strong negative correlation was found between *EGFR* and *BRG1* expression in the Director's Challenge data set (Fig. 4a). When comparing gene expression of *EGFR* and *BRG1* mutant cell lines to WT lines, *EGFR* was the first of 21 shared upregulated genes, overexpressed 3.1-fold in *BRG1* mutant cell lines and 3.25-fold in *EGFR* mutant cell lines (Extended Data Fig. 7b, c and Supplementary Table 5).

To understand their genetic relationship better, EGFR and BRG1 expressions were manipulated (Fig. 4b and Extended Data Fig. 8a). BRG1 re-expression in the HCC15 lines converted the line from a sensitized to protected phenotype, and the HCC15 shEGFR line was no longer sensitized to etoposide by DZNep (Fig. 4c). Similarly, DZNep had no effect on etoposide IC_{50} when EGFR was overexpressed or BRG1 was knocked down in H460 cells (Fig. 4c). These changes in etoposide sensitivity were

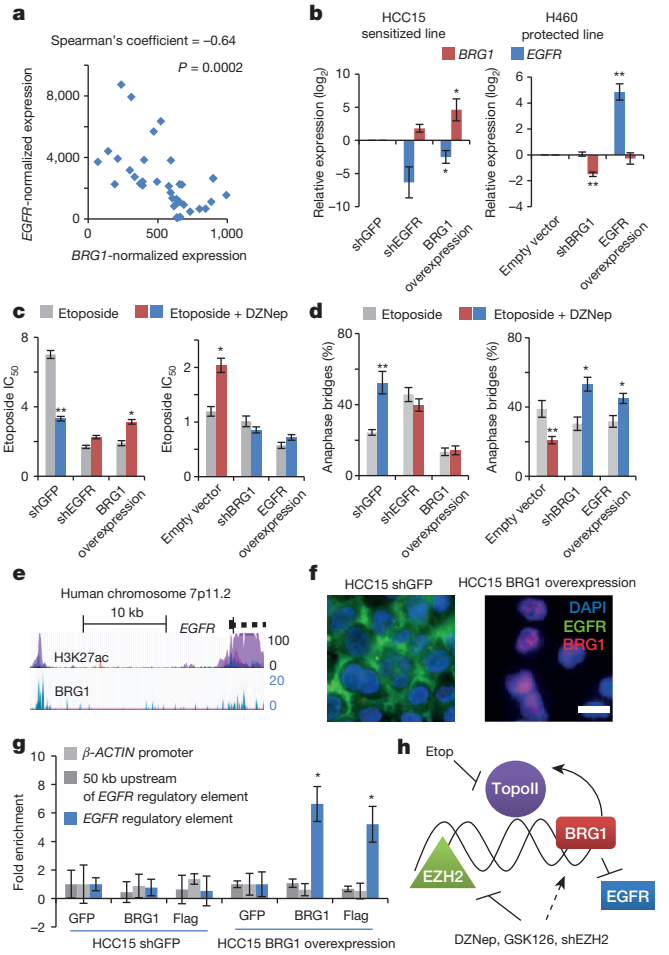

Figure 4 | BRG1 and *EGFR* are genetically antagonistic and control the sensitized phenotype. **a**, *EGFR* and *BRG1* expression in tumours from the Director's Challenge were plotted and correlation was assessed ($n = 36$). **b**, RT-qPCR for average expression of *BRG1* and *EGFR* ± s.e.m. in indicated transduced HCC15 and H460 cell lines ($^*P < 0.04$, $^{**}P < 0.0001$; $n = 5$ biological replicates for H460, $n = 4$ biological replicates for HCC15). **c**, Average etoposide IC_{50} ± s.e.m. in the indicated vehicle- and DZNep-treated cells ($n = 3$ biological replicates; $^*P < 0.04$, $^{**}P < 0.0001$). **d**, Average percentage of anaphase structures with bridges ± s.e.m. in indicated vehicle- or DZNep-treated cell lines ($n = 3$ biological replicates; $^*P < 0.04$, $^{**}P < 0.02$). **e**, Depiction of EGFR regulatory element including H3K27ac and BRG1 binding peaks and from ENCODE database. **f**, Immunofluorescence for EGFR and BRG1 on HCC15 cells transduced with short hairpin targeting green fluorescent protein (shGFP, control) and BRG1-overexpressing HCC15 cells; scale bar, 30 μm. **g**, Chromatin immunoprecipitation for GFP (control), BRG1 or the Flag-tag on the exogenously expressed BRG1 in the HCC15 shGFP (control) and BRG1-expressing cell lines. qPCR was performed with primers for indicated genomic sites and average enrichment over GFP ± s.e.m. was plotted ($n = 4$ biological replicates, one-way analysis of variance; $^*P = 0.02$). **h**, In response to EZH2i: WT cells show increased BAF complex function and subsequent decrease in etoposide sensitivity; *BRG1* mutant cells have increased etoposide sensitivity; and EGFR mutant cells act like *BRG1* mutant cells owing to genetic antagonism of *EGFR* by BRG1.

consistent with changes in anaphase bridging, apoptosis and S phase accumulation (Fig. 4d and Extended Data Fig. 8b, c).

The ENCODE database[18] shows a chromatin immunoprecipitation peak for BRG1 upstream of *EGFR* (Fig. 4e). HCC15 cells re-expressing BRG1 had lower levels of EGFR by RT-qPCR and immunofluorescence (Fig. 4b, f). We hypothesized that BRG1-containing BAF complexes bind to the *EGFR* regulatory element to disrupt *EGFR* transcription, as observed in other systems[19]. We confirmed the exogenously expressed BRG1 was being incorporated into BAF complexes (Extended Data Fig. 9a), and then performed chromatin immunoprecipitation assays. BRG1, immunoprecipitated with an antibody recognizing the protein itself or the Flag-tag, was significantly associated with the *EGFR* regulatory element (Fig. 4g). This genetic antagonism explains why dividing cells in *EGFR*-driven cultures may not sufficiently upregulate BRG1, and respond to combined etoposide and EZH2i with increased anaphase bridging as *BRG1* mutant cells do (Fig. 4h).

Our results suggest that dual EZH2i plus TopoIIi represents a treatment option for *EGFR* mutant tumours, even those that invariably develop resistance to EGFR tyrosine-kinase inhibitors[12]. Furthermore, combination EZH2i plus TopoIIi offers the first specific therapeutic for *BRG1* mutant lung cancers. Importantly, the strong antagonism of etoposide and EZH2i warns against using this drug combination for EGFR and BRG1 WT tumours. Also notable is the fact that EZH2i either sensitized to etoposide (synergism) or protected from it (antagonism), but very rarely was additivity observed. We and others[20,21] have found that *BRG1* and *EGFR* mutations are significantly anti-correlated in NSCLC. Moreover, *BRG1* mutant NSCLCs had elevated *EGFR* levels, raising the possibility that *BRG1* mutant tumours represent a subset of patients with WT EGFR that respond to EGFR tyrosine-kinase inhibitor[20,21]. Unlike *Brg1*-deficient MEFs[14], *BRG1* mutant lung cancer cells did not exhibit TopoII dysfunction unless EZH2 was inhibited, suggesting a novel connection between EZH2 and TopoII function.

Online Content Methods, along with any additional Extended Data display items and Source Data, are available in the online version of the paper; references unique to these sections appear only in the online paper.

Received 13 November 2013; accepted 26 November 2014.
Published online 28 January 2015.

1. Jemal, A. *et al.* Global cancer statistics. *CA Cancer J. Clin.* **61,** 69–90 (2011).
2. Zornosa, C. *et al.* First-line systemic therapy practice patterns and concordance with NCCN guidelines for patients diagnosed with metastatic NSCLC treated at NCCN institutions. *J. Natl. Compr. Canc. Netw.* **10,** 847–856 (2012).
3. Wang, L. *et al.* Randomized phase II study of concurrent cisplatin/etoposide or paclitaxel/carboplatin and thoracic radiotherapy in patients with stage IIIl non-small cell lung cancer. *Lung Cancer* **77,** 89–96 (2012).
4. Baylin, S. B. & Jones, P. A. A decade of exploring the cancer epigenome – biological and translational implications. *Nature Rev. Cancer* **11,** 726–734 (2011).
5. Simon, J. A. & Lange, C. A. Roles of the EZH2 histone methyltransferase in cancer epigenetics. *Mutat. Res.* **647,** 21–29 (2008).
6. Shedden, K. *et al.* Gene expression-based survival prediction in lung adenocarcinoma: a multi-site, blinded validation study. *Nature Med.* **14,** 822–827 (2008).
7. Tan, J. *et al.* Pharmacologic disruption of Polycomb-repressive complex 2-mediated gene repression selectively induces apoptosis in cancer cells. *Genes Dev.* **21,** 1050–1063 (2007).
8. Choudhury, S. R. *et al.* (-)-Epigallocatechin-3-gallate and DZNep reduce polycomb protein level via a proteasome-dependent mechanism in skin cancer cells. *Carcinogenesis* **32,** 1525–1532 (2011).
9. McCabe, M. T. *et al.* EZH2 inhibition as a therapeutic strategy for lymphoma with EZH2-activating mutations. *Nature* **492,** 108–112 (2012).
10. Chou, T. & Talalay, P. Quantitative analysis of dose-effect relationships: the combined effects of multiple drugs of enzyme inhibitors. *Adv. Enzyme Regul.* **22,** 27–55 (1984).
11. Deweese, J. E. & Osheroff, N. The DNA cleavage reaction of topoisomerase II: wolf in sheep's clothing. *Nucleic Acids Res.* **37,** 738–748 (2009).
12. Ji, H. *et al.* The impact of human EGFR kinase domain mutations on lung tumorigenesis and *in vivo* sensitivity to EGFR-targeted therapies. *Cancer Cell* **9,** 485–495 (2006).
13. Jackson, E. L. *et al.* The differential effects of mutant p53 alleles on advanced murine lung cancer. *Cancer Res.* **65,** 10280–10288 (2005).
14. Dykhuizen, E. C. *et al.* BAF complexes facilitate decatenation of DNA by topoisomerase II. *Nature* **497,** 624–627 (2013).
15. Wilson, B. G. *et al.* Epigenetic antagonism between Polycomb and SWI/SNF complexes during oncogenic transformation. *Cancer Cell* **18,** 316–328 (2010).
16. Imielinski, M. *et al.* Mapping the hallmarks of lung adenocarcinoma with massively parallel sequencing. *Cell* **150,** 1107–1120 (2012).
17. TCGA. Comprehensive molecular profiling of lung adenocarcinoma. *Nature* **511,** 543–550 (2014).
18. ENCODE. An integrated encyclopedia of DNA elements in the human genome. *Nature* **489,** 57–74 (2013).
19. Hargreaves, D. C. & Crabtree, G. R. ATP-dependent chromatin remodeling: genetics, genomics and mechanisms. *Cell Res.* **21,** 396–420 (2011).
20. Oike, T. *et al.* A synthetic lethality-based strategy to treat cancers harboring a genetic deficiency in the chromatin remodeling factor BRG1. *Cancer Res.* **73,** 5508–5518 (2013).
21. Matsubara, D. *et al.* Lung cancer with loss of BRG1/BRM, shows epithelial mesenchymal transition phenotype and distinct histologic and genetic features. *Cancer Sci.* **104,** 266–273 (2013).

Supplementary Information is available in the online version of the paper.

Acknowledgements We thank the Kim laboratory, F. Luo, P. Louis, K. Harrington, X. Wang and J. Brainson for technical assistance and discussions, and J. Crabtree, D. Hargreaves, C. Kadoch, L. Zon, K. Cichowski, M. Enos, S. Orkin, A. Gutierrez and C. Roberts for discussions. This work was supported in part by the Ladies Auxiliary to the Veterans of Foreign Wars, PF-12-151-01-DMC from the American Cancer Society, and the Uniting Against Lung Cancer Young Investigator Award supported by Meryl Bralower (C.M.F.), Boston University Undergraduate Research Opportunities Program (P.T.D.), RO1 HL090136, U01 HL100402 RFA-HL-09-004, American Cancer Society Research Scholar Grant RSG-08-082-01-MGO, the V Foundation for Cancer Research, a Basil O'Conner March of Dimes Starter Award, the Harvard Stem Cell Institute, and the Lung Cancer Research Foundation (C.F.K.), the National Institutes of Health (NIH) grants CA122794, CA140594, CA163896, CA166480, CA154303 and CA120964 (K.K.W.), the Intramural Research Program of the NIH, National Cancer Institute, Center for Cancer Research (V.E.M.), and the NIH grant K08 CA163677 (P.S.H.).

Author Contributions C.M.F., C.X., K.K.W. and C.F.K. designed the study; C.M.F., C.X., P.T.J., J.M.B. and Y.J.L. performed the experiments; S.P.R. cloned the EZH2 complementary DNA (cDNA) vector; H.Z. performed EZH2 immunohistochemistry, V.E.M. provided DZNep, P.S.H. analysed primary tumour sequencing data; K.K.W. allowed autochthonous mouse models studies in his laboratory; C.M.F. and C.F.K. wrote the manuscript with comments from all authors.

Author Information Reprints and permissions information is available at www.nature.com/reprints. The authors declare no competing financial interests. Readers are welcome to comment on the online version of the paper. Correspondence and requests for materials should be addressed to C.F.K. (carla.kim@childrens.harvard.edu).

METHODS

Cell lines. Cell lines used are listed in Supplementary Table 4. All cell lines were maintained in RPMI 1640 media with 10% fetal bovine serum, 4 mM L-glutamine and penicillin/streptomycin at 37 °C, 5% CO_2. Cell lines were obtained from the Meyerson laboratory at Dana-Farber Cancer Institute. No mycoplasma was detected in cultures by either routine mycoplasma PCR or perinuclear 4′,6-diamidino-2-phenylindole (DAPI) staining. Cell line genotypes (Supplementary Table 4) were obtained from published studies[22,23], COSMIC database[24] and CCLE database[25].

Vectors. The pLKO.1 EZH2 shRNA construct clones TRCN0000040076 and TRCN0000040073 were purchased from Sigma and the shGFP plasmid 12273 is available on Addgene[26]. Both shBRG1 and the matched empty vector were provided by the Smale laboratory[27] and are available on Addgene, the BRG1 overexpression plasmid 19148 from the Massagué laboratory[28] was purchased through Addgene, and the shEGFR and EGFR WT overexpression constructs were provided by the Jänne laboratory[29]. The EZH2 overexpression construct was derived by cloning human EZH2 cDNA into pLenti7.3/V5-DEST (Invitrogen). Lentivirus was packaged in HEK293T cells using established protocols[30], and retrovirus was packaged in PlatE cells again using established protocols[31]. Cell lines were infected with viral-containing supernatant containing 6 μg ml^{-1} polybrene (Sigma) for a period of 10–18 h. Infected cultures were selected with 1 μg ml^{-1} puromycin (all sh constructs and EGFR overexpression, SIMGA), 200 μg ml^{-1} hygromycin (BRG1 overexpression, Invitrogen), or by flow cytometry for GFP (EZH2 overexpression) 5 days after infection.

Small hairpin sequences: GFP: GCCC(GCAAGCTGACCCTGAAGTTCAT)TCAAGAG(ATGAACTTCAGGGTCAGCTTGC)TTTT; EZH2 coding region: CCGG(CGGAAATCTTAAACCAAGAAT)CTCGAG(ATTCTTGGTTTAAGATTTCCG)TTTTT; EZH2 3′ UTR: CCGG(TATTGCCTTCTCACCAGCTGC)CTCGAG(GCAGCTGGTGAGAAGGCAATA)TTTTT; EGFR: CCGG(GCTGAGAATGTGGAATACCTA)CTCGAG(TAGGTATTCCACATTCTCAGC)TTTTT; BRG1: TTTG(TGGATAAGCAGCACAAGATT)TCAAGAG(AATCTTCTGCTGCTTCTCCA)TTTTT.

Drugs. Etoposide and doxorubicin (Sigma) were diluted to a stock of 100 mM in dimethyl sulphoxide (DMSO) for all cell culture experiments. DZNep was a gift from V.E.M. and was diluted in DMSO to a stock of 10 mM. GSK126 was purchased from Xcess Bio as a 10 mM stock in DMSO. All stocks were diluted in DMSO to 1,000× concentration before addition into media at 2× concentration and final dilution onto plated cells 1:1.

Cytotox assays. Cell lines were dissociated, counted and plated at 5,000 cells per well in flat-bottomed opaque tissue-culture-treated 96-well plates (CytoOne). Edge wells were filled with PBS. The following day, 2× drug diluted in media was added to each well such that the well then contained 100 μl media with 1× drug concentration at the following doses: etoposide, 0, 0.1, 1, 3, 5, 7, 10, 50, 100, 500 μM; or doxorubicin, 0, 0.01, 0.1, 0.5, 1, 3, 5, 7, 10, 50 μM; with or without additional 1 μM DZNep, 10 μM GSK126 or a continuation of 2 μM GSK126 from a 9-day 2 μM GSK126 pretreated culture. After 4 days, CellTiter-Glo (Promega) was added and luminescence was read on a BioTec plate reader to determine relative cell number in each well. Data were averaged for triplicate or quadruplicate technical replicates and normalized to the untreated wells, and whole runs (vehicle and EZH2i) were excluded if vehicle-treated wells did not reach the threshold luminescence of 3,000. Results from independent biological replicate experiments were input into GraphPad Prism software to extrapolate the IC_{50} and s.e.m. of IC_{50} for a given cell line using the nonlinear regression analysis of log(inhibitor) versus normalized response with a variable slope. For 1 μM DZNep for 4 days with etoposide, $n = 3$ biological replicates for H1975, H2030, HCC4006, A549, HCC2450, Calu1, H1650, H522, H2126, H1299, HCC15, H322, H2009, HCC95, H520, H460, Calu3, H2122, H23 and H3255; $n = 4$ biological replicates for PC9, H157, HCC827, Sw1573, Calu6 and H441. For both 2 μM GSK126 pretreated for 9 days and continued for 4 days with etoposide, and 10 μM GSK126 treated for 4 days with etoposide, $n = 3$ biological replicates. The log(IC_{50}) values were compared using GraphPad Prism software, and P values reported are the sum-of-squares F statistics. For graphs, log(IC_{50}) of vehicle control cells was subtracted from log(IC_{50}) of EZH2i-treated cells and multiplied by ten to be depicted as log fold change × 10. Errors were estimated by calculating possible upper and lower bounds of log fold changes based on GraphPad reported s.e.m. for each log(IC_{50}) calculated.

For Chou–Talalay combination index assays[10], doses for etoposide, DZNep or GSK126 were 0, 0.1, 0.5, 1, 3, 5, 7, 10, 30, 50 μM and 1:1 combinations of etoposide and DZNep or etoposide and GSK126. Survival percentages for three independent biological replicate experiments were averaged and input into CompuSyn software to extrapolate combination index values. Any drug dose with mean survival over 100% was excluded because the CompuSyn software did not allow for values over 1. In addition, visual inspection led us to remove the highest doses of GSK126 from the analysis for every cell line, as suggested in refs 32 and 33, leading to much better matching of the data points to the median effect plot. Notably, removal of these data points both increased synergy seen in the sensitized lines and increased antagonism seen in H460 and Sw1573 lines.

Flow cytometry. For 7AAD-cell cycle analysis, cell lines were plated at 1.5×10^6 cells per 10 cm plate and treated with drug for 4 days. Cells were then dissociated, fixed with 100% ice cold ethanol for at least 2 h, incubated for 30 min with 1 mg ml^{-1} DNase-free RNase A (Thermo) and resuspended in 20 μg ml^{-1} 7-aminoactinomycin D (7AAD; Invitrogen). Thirty thousand events were collected on the BD Fortessa, analysed with ModFit LT software and the results were averaged for three or four biological replicates (n indicated in legend).

For Annexin V/7AAD apoptosis analysis, cell lines were plated at 5×10^4 cells per well of a six-well plate and treated with drug for 3 days. Supernatant was retained and added to trypsinized suspensions of adherent cells. Cells were stained with Annexin V-FITC (BD Biosciences) according to the manufacturer's instructions, and resuspended with 1 μg ml^{-1} 7AAD before analysis on BD Fortessa. For sensitized lines 2 μM GSK126 pretreated for 9 days and continued for 3 days with etoposide was used, while for protected line 10 μM GSK126 treated for 3 days with etoposide was used. Data were analysed with FlowJo (Treestar) software and the percentages of Annexin V^+/$7AAD^-$ cells were averaged for four biological replicate experiments.

Quantitative RT–PCR. RNA from treated cell lines was extracted using Absolutely RNA kits (Agilent) and cDNA was made using the SuperScript III kit (Invitrogen). Relative gene expression was assayed with Sybr green on the StepOnePlus real-time PCR system (Applied Biosystems). Relative expression was calculated by using threshold cycle (C_t) values: gene of interest($C_{t,\ \mathrm{reference}} - C_{t,\ \mathrm{experimental}}$) − CYPA($C_{t,\ \mathrm{reference}} - C_{t,\ \mathrm{experimental}}$) and graphs potted on the $\log_2$ scale or converted to linear scale. Statistics were performed on $\log_2$ data. For all experiments, the reference sample was a matched vehicle-treated or control transduced cell line.

Primer sequences: CYPA: F TCATCTGCACTGCCAAGACTG R CATGCCTTCTTTCACTTTGCC; EZH2: F AGGAGTTTGCTGCTGCTCTC R CCGAGAATTTGCTTCAGAGG; BRG1: F AGCGATGACGTCTCTGAGGT R GTACAGGGACACCAGCCACT; EGFR: F TAACAAGCTCACGCAGTTGG R GTTGAGGGCAATGAGGACAT.

Xenograft experiments. For DZNep experiments, H157 or H23 cells were dissociated into single cells, counted and resuspended at 1×10^6 cells per 250 μl of 1:1 media/matrigel (BD). Eight- to 16-week-old female Foxn1^{nu}/Foxn1^{nu} (Nude) mice (Harlan) were injected subcutaneously with 1×10^6 cells in two to four spots on flanks. Etoposide and DZNep were administered from day 12 to day 17 after injections; etoposide: 20 mg/kg/d intraperitoneally in corn oil once per day for 5 consecutive days; DZNep 2 mg/kg/d intraperitoneally in corn oil twice per week for 1 week, or 1 mg/kg/d intraperitoneally in corn oil twice per week for 2 weeks. Tumour growth was measured every other day by calliper in a non-blinded fashion. For GSK126 experiments, PC9 cells were dissociated into single cells, counted and resuspended at 1×10^6 cells per 250 μl of 1:1 media/matrigel (BD). Eight- to 16-week-old female Foxn1^{nu}/Foxn1^{nu} mice (Harlan) were injected subcutaneously with 1×10^6 cells in one spot on left flank. Tumours were allowed to grow for 23 days to a mean size of 70 mm^3. Mice were then randomized into groups that received etoposide, GSK126, both etoposide and GSK126, gefitinib or vehicle: etoposide 10 mg/kg/d intraperitoneally in corn oil three times a week, GSK126 300 mg/kg/d intraperitoneally in 1:1 v/v GSK126/Captisol mixture resuspended in sterile water with acetic acid to pH 4.8, gefitinib (LC Laboratories) 150mg/kg/d in 1% Tween-80 (Sigma). All mouse experiments were approved by the BCH Animal Care and Use Committee and by the Dana-Farber Cancer Institute Institutional Animal Care and Use Committee, both accredited by the Association for Assessment and Accreditation of Laboratory Animal Care, and were performed in accordance with relevant institutional and national guidelines and regulations.

Generation of the EZH2 co-expression gene signature. We used Oncomine[34] to query the top 20 genes co-expressed with EZH2 in all data sets containing human non-small-cell lung cancer samples and co-expression data[6,35–41]. We chose 20 probes for examination from each study, to yield a list between 100 and 200 genes, which allowed for robust hierarchal clustering of samples similar to that in previous studies. Of the 180 probes, 64 were redundant, leading to a list of 116 genes highly co-expressed with EZH2 (Supplementary Table 1). Because these data sets were from various microarray platforms, the gene list was then used to generate a probe list for the 116 genes corresponding to probes on the U133A Affymetrix array using the batch query function on the NetAffx website (http://www.affymetrix.com/analysis/index.affx). Gene ontology analysis was performed on the *EZH2* co-expression signature with dChip software (http://www.hsph.harvard.edu/cli/complab/dchip/).

Microarray analysis. All array data are publically available on Gene Expression Omnibus (http://www.ncbi.nlm.nih.gov/geo/) and correspond to array files available from GSE4824 (ref. 42) for all lines except A549, H522 and PC9, GSE5457 for A549 (two replicates), GSE5720 (ref. 43) for H522 and an additional A549, GSE7670 (ref. 44) for an additional H1299, GSE10089 (ref. 45) for PC9 and H1650, and

GSE31625 (ref. 46) for an additional PC9. Arrays were chosen based on availability in September 2012. Arrays were analysed using R/Bioconductor (http://www.bioconductor.org/). Raw CEL files from U133A Affymetrix arrays were processed using the robust multiarray average algorithm[47]. To identify genes correlating with the phenotypic groups, we used limma[48] to fit a statistical linear model to the data and then tested for differential gene expression in the three groups using the vennSelect package—WT: H460, H441, H2122, H2009, Calu6, HCC95; EGFR mutant: H1650, HCC827, HCC4006, H1975, H3255, PC9; BRG1 mutant: A549, H1299, H157, H2126, H522, HCC15. Results were adjusted for multiple testing using the Benjamini and Hochberg method[49], and significance was determined using a false-discovery-rate cutoff of less than 5%. For correlation between *EGFR* and *BRG1* expression in the Director's Challenge data set, the arrays were processed using RMA and limma as described above. Tumours with a robust multiarray average normalized expression of more than 2,000 for *EGFR* or 575 for *BRG1* were plotted and correlation was assessed—because these data were nonparametric, Spearman's correlation coefficient was used. Using this same method of selecting for highest-expressing tumours, we could visualize positive correlations between *EZH2* and other *EZH2* co-expression gene signature members (data not shown).

Kaplan–Meier analysis. Raw gene expression data from the Director's Challenge human lung adenocarcinoma samples[6] were obtained (https://caintegrator.nci.nih.gov/caintegrator/). Probe intensities from the Affymetrix U133A platform used in these studies were normalized and modelled using dChip software[50] (http://www.hsph.harvard.edu/cli/complab/dchip/). Kaplan–Meier survival analyses were implemented after the samples were hierarchically clustered using centroid linkage, rank correlation and gene peaking time into two risk groups using the EZH2 co-expression gene signature. Survival differences between the two risk groups were assessed using the Mantel–Haenszel log-rank test. The large area between the two risk groups and its associated small *P* value from the Mantel–Haenszel log-rank test implicate a robust survival classification model.

Statistical analysis. No statistical methods were used to predetermine sample size. Except where indicated, a two-tailed Student's *t*-test with equal variance was used to compare measurements between two conditions with at least three biological replicates per condition. Normal distribution was checked with the Kolmogorov–Smirnov test; data that failed the test at $\alpha = 0.05$ were considered normally distributed. If the data were non-parametric, then a two-tailed Mann–Whitney *U*-test was used instead of a *t*-test to assess the *P* value. Unless noted otherwise, pooled data are represented by the mean and standard error. *P* values are indicated in figure legends, and *P* values less than 0.05 were considered significant.

Western blot. Whole-cell extracts were made in RIPA buffer (0.5% Deoxycholate, 1% IGEPAL-CA630, 0.1% sodium dodecyl sulphate, 150 mM NaCl, 50 mM Tris-8.1), lysates were cleared by centrifugation, and protein concentrations were quantified with the Pierce BCA Protein Assay Kit (Thermo). For western blotting, 25 μg of protein extract per sample was denatured with heat and reducing agents, separated on a 4–12% acrylamide gel (BioRad) and transferred to nitrocellulose (GE Healthcare). Antibodies used for western blotting were as follows: EZH2 (clone D2C9; Cell Signaling; 1:200), Histone H3 (polyclonal; AbCAM ab1791; 1:2,000) and H3K27me3 (polyclonal; Millipore 07-449; 1:1,000), all incubated overnight at 4 °C. All antibodies have detailed species validation available online from vendors. Secondary antibody, anti-rabbit-HRP (Santa Cruz sc-2313; 1:10,000), was incubated for 1 h at room temperature. After washing, chemiluminescence was visualized with Western Lightning Plus-ECL (PerkinElmer) and exposure onto KODAK BioMax XAR film.

Immunoprecipitation. Cultured cells (10×10^6 per line) were collected by trypsinization and pelleting, followed by PBS wash and pelleting. On ice, cell pellets were resuspended in 750 μl hypotonic buffer (10 mM Tris-HCl, pH 7.4, 10 mM NaCl, 3 mM $MgCl_2$) and incubated for 15 min. NP-40 (10%, 37.5 μl) was added to each tube followed by vortexing for 10 s and centrifugation for 10 min at 650*g* at 4 °C. Nuclear pellets were then resuspended in RIPA buffer for 30 min on ice with vortexing, lysates were cleared by centrifugation and protein concentrations were quantified with the Pierce BCA Protein Assay Kit (Thermo). Antibodies directed against Flag (M2; Sigma; 1:50), BAF155 (R-18; Santa Cruz; 1:50) or ARID1a (PSG3; Santa Cruz; 1:10) were incubated with 300 μg of each nuclear extract with 1:1 Protein A and Protein G agarose beads (GE Healthcare) rotating at 4 °C overnight. All antibodies had detailed species validation available online from vendors. Beads were washed three times in 1 ml RIPA buffer with the second wash being rotated at 4 °C for 30 min, then resuspended in approximately 35 μl 1× reducing buffer and boiled for 5 min before loading 10 μl per lane. Proteins were separated on a 4–12% acrylamide gel (BioRad) and transferred to nitrocellulose (GE Healthcare). Antibodies for western blotting were as follows: Flag (M2; Sigma; 1:1,000), BAF155 (R-18; Santa Cruz; 1:1,000) and ARID1a (polyclonal; Bethyl Laboratories A310-040A; 1:1,000). Secondary antibody, anti-rabbit-HRP (Santa Cruz sc-2313; 1:10,000), anti-mouse-HRP (Santa Cruz sc-2314; 1:10,000) or anti-goat-HRP (Santa Cruz sc-2020; 1:10,000) were incubated for 1 h at room temperature. After washing, chemiluminescence was visualized with Western Lightning Plus-ECL (PerkinElmer) and exposure onto KODAK BioMax XAR film.

Anaphase bridge analysis. To quantify anaphase bridges, cells were grown on four-well cultures slides (Lab Tek II). Adherent cells were fixed with 4% paraformaldehyde for 20 min, washed and stained with Vectashield with DAPI (Vector Labs). Images were taken of each anaphase structure, and the number of anaphases with bridges over the total number of anaphases (between 11 and 34 total anaphases per well of a four-well chamber slide) was recorded for each of three or more independent biological replicate experiments in a blinded fashion. Exact biological replicates *n* for Fig. 3b were as follows: PC9 vehicle = 7, DZNep = 4, GSK126 = 4; A549 vehicle = 3, DZNep = 3, GSK126 = 3; H157 vehicle = 7, DZNep = 5, GSK126 = 3; H23 vehicle = 6, DZNep = 4, GSK126 = 3; Sw1573 vehicle = 4, DZNep = 4, GSK126 = 3; and for Extended Data Fig. 5b were H441 vehicle = 3 DZNep = 3; H2009 vehicle = 3, DZNep = 3; H522 vehicle = 3, DZNep = 3; and H1650 vehicle = 4, DZNep = 4. Imaging was performed with a Nikon 90i camera with ×100 objective and oil emersion and NIS-Elements software, and processed with NIS-Elements and Adobe Photoshop.

Immunofluorescence. Cells were fixed in 4% paraformaldehyde and permeabilized with 10% Normal Donkey Serum (Jackson Immunoresearch), 0.25% Triton-X (Sigma), both in PBS. Primary antibodies, Brg1 (clone G-7, Santa Cruz) and EGFR (polyclonal; Cell Signaling 2232) were incubated overnight at 1:100 dilution in PBS, 10% Normal Donkey Serum. All antibodies had detailed species validation available online from vendors. Slides were washed three times and secondary antibodies, anti-mouse-AlexaFluor594 and anti-rabbit-AlexaFluor488 (Invitrogen) were incubated at 1:500 for 1 h. After washing, cover slips were mounted with Vectashield with DAPI (Vector Labs). Imaging was performed with a Nikon 90i camera and NIS-Elements software, and processed with NIS-Elements and Adobe Photoshop. All treatment groups were imaged with the same exposure time and equivalent processing. Images were chosen to highlight the difference between $BRG1^{high}$ interphase cells and $EGFR^{high}$ dividing cells in EZH2i-treated PC9 cultures.

Treatment and magnetic resonance imaging of endogenous mouse models. Doxycycline-inducible $EGFR^{T790M;L858R}$ transgenic mice[12] and *Lox-Stop-Lox-*$Kras^{G12D/+}$;$p53^{fl/fl}$ ($Kras^{G12D/+}$;$p53^{\Delta/\Delta}$)[13,51] mice were maintained on a mixed background, housed in a pathogen-free environment at the Harvard School of Public Health and handled in strict accordance with Good Animal Practice as defined by the Office of Laboratory Animal Welfare. All animal work was done with Dana-Farber Cancer Institute Institutional Animal Care and Use Committee approval. Cohorts of male and female $EGFR^{T790M;L858R}$;CCSP-rtTA were put on a doxycycline diet at 6 weeks of age to induce the expression of mutant EGFR, while male and female $Kras^{G12D/+}$;$p53^{\Delta/\Delta}$ mice received intranasal adeno-Cre between 6 and 8 weeks of age. Mice were evaluated by magnetic resonance imaging 12–16 weeks after doxycycline diet or adeno-Cre infection to document and quantify the lung cancer burden before being randomized to various treatment study cohorts. Treated mice in all cohorts had similar initial tumour burden. Tumour-bearing mice were randomized into cohorts treated either with vehicle (corn oil), etoposide 10 mg/kg intraperitoneally three times a week for 4 weeks, DZNep 4 mg/kg intraperitoneally twice a week for 4 weeks or both etoposide and DZNep. The mice were imaged by magnetic resonance imaging every 2 weeks to determine the reduction in tumour volume during the respective treatments as described previously in a non-blinded fashion[12]. The tumour burden volume and quantification were reconstructed on three-dimensional slicer software (http://www.slicer.org). Immunohistochemistry was performed as described with anti-EZH2 (clone D2C9; Cell Signaling) or anti-pEGFR (Y1068; clone D7A5; Cell Signaling) and developed using Vectastain Elite ABC kit (Vector Labs). Imaging was performed with a Nikon 90i camera and NIS-Elements software, and processed with NIS-Elements and Adobe Photoshop.

Chromatin immunoprecipitation. Five million cells were fixed in 1% formaldehyde for 10 min before addition of glycine to a concentration of 1 mM. Cells were pelleted, washed and resuspended in chromatin immunoprecipitation sonication buffer (1% Triton X-100, 0.1% deoxycholate, 50 mM Tris 8.1, 150 mM NaCl, 5 mM EDTA) containing protease and phosphastase inhibitors (Roche). Samples were sonicated for a total of 3 min in 30 s cycles with 1 min breaks. Sonicated samples were centrifuged for 15 min to clear the lysates, and resulting whole-cell extracts were used for pull-downs. Antibodies directed against GFP (Ab-1; Neomarkers), BRG1 (G-7; Santa Cruz) and Flag (M2; Sigma) were incubated with equal proportions of whole-cell extracts at 1:30 dilution overnight, rotating at 4 °C. Protein A and Protein G agarose beads (1:1; GE Healthcare) were added and incubated for 2 h at 4 °C. Beads were then pelleted and washed with high salt wash buffer (1% Triton X-100, 0.1% deoxycholate, 50 mM Tris-8.1, 500 mM NaCl, 5 mM EDTA), followed by LiCl immune complex buffer (250 mM LiCl, 0.5% IGEPAL-CA630, 0.5% deoxycholate, 10 mM Tris-8.1, 1 mM EDTA) and TE (10 mM Tris-8.1, 1 mM EDTA) before suspension in elution buffer (1% SDS, 0.1 M $NaHCO_2$, 0.01 mg ml^{-1} salmon sperm DNA (GE Healthcare)). Crosslinks were reversed at 65 °C overnight, beads were pelleted, and resulting supernatant was incubated with 0.4 mg ml^{-1} Proteinase K (Sigma) for

2 h at 37 °C. DNA from each sample was purified using Qiagen PCR purification columns following the manufacturer's instructions. Samples were resuspended in 100 µl 10 mM Tris-8.1 and 2 µl were used for each Sybr green PCR reaction (Applied Biosystems). Enrichment was calculated by average ($C_{t,\ reference} - C_{t,\ experimental}$) and converted to the linear scale for each genomic region of interest. Reference samples were the GFP; both BRG1 and Flag samples were experimental. Statistical analyses (one-way analysis of variance) were performed on $\log_2$-transformed data for three independent biological replicates.

Primer sequences: β-actin: F TCGAGCCATAAAAGGCAACT R TCTCCCTC CTCCTCTTCCTC; EGFR regulatory element: F CCTTGTAGATTGGGGCTGA G R AGTTTGGGGGTGGAAGAAAG; 50kb upstream of regulatory element: F GGCTGAGACAGAGGGAACAC R CCATCTCAGCCTCCCAAGTA.

22. Medina, P. P. *et al.* Frequent BRG1/SMARCA4-inactivating mutations in human lung cancer cell lines. *Hum. Mutat.* **29,** 617–622 (2008).
23. Yamamoto, H. *et al.* PIK3CA mutations and copy number gains in human lung cancers. *Cancer Res.* **68,** 6913–6921 (2008).
24. Bamford, S. *et al.* The COSMIC (Catalogue of Somatic Mutations in Cancer) database and website. *Br. J. Cancer* **91,** 355–358 (2004).
25. Barretina, J. *et al.* The Cancer Cell Line Encyclopedia enables predictive modelling of anticancer drug sensitivity. *Nature* **483,** 603–607 (2012).
26. Orimo, A. *et al.* Stromal fibroblasts present in invasive human breast carcinomas promote tumor growth and angiogenesis through elevated SDF-1/CXCL12 Secretion. *Cell* **121,** 335–348 (2005).
27. Ramirez-Carrozzi, V. R. *et al.* Selective and antagonistic functions of SWI/SNF and Mi-2 nucleosome remodeling complexes during an inflammatory response. *Genes Dev.* **20,** 282–296 (2006).
28. Xi, Q., He, W., Zhang, X. H.-F., Le, H.-V. & Massagué, J. Genome-wide impact of the BRG1 SWI/SNF chromatin remodeler on the transforming growth factor β transcriptional program. *J. Biol. Chem.* **283,** 1146–1155 (2008).
29. Engelman, J. A. *et al.* Allelic dilution obscures detection of a biologically significant resistance mutation in EGFR-amplified lung cancer. *J. Clin. Invest.* **116,** 2695–2706 (2006).
30. Fillmore, C. M. *et al.* Estrogen expands breast cancer stem-like cells through paracrine FGF/Tbx3 signaling. *Proc. Natl Acad. Sci. USA* **107,** 21737–21742 (2010).
31. Zacharek, S. J. *et al.* Lung stem cell self-renewal relies on bmi1-dependent control of expression at imprinted loci. *Cell Stem Cell* **9,** 272–281 (2010).
32. Chou, T.-C. Drug combination studies and their synergy quantification using the Chou-Talalay method. *Cancer Res.* **70,** 440–446 (2010).
33. Chou, T.-C. Theoretical basis, experimental design, and computerized simulation of synergism and antagonism in drug combination studies. *Pharmacol. Rev.* **58,** 621–681 (2006).
34. Rhodes, D. R. *et al.* Oncomine 3.0: genes, pathways, and networks in a collection of 18,000 cancer gene expression profiles. *Neoplasia* **9,** 166–180 (2007).
35. Beer, D. G. *et al.* Gene-expression profiles predict survival of patients with lung adenocarcinoma. *Nature Med.* **8,** 816–824 (2002).
36. Garber, M. E. *et al.* Diversity of gene expression in adenocarcinoma of the lung. *Proc. Natl Acad. Sci. USA* **98,** 13784–13789 (2001).
37. Gordon, G. J. *et al.* Translation of microarray data into clinically relevant cancer diagnostic tests using gene expression ratios in lung cancer and mesothelioma. *Cancer Res.* **62,** 4963–4967 (2002).
38. Landi, M. T. *et al.* Gene expression signature of cigarette smoking and its role in lung adenocarcinoma development and survival. *PLoS ONE* **3,** e1651 (2008).
39. Rohrbeck, A. *et al.* Gene expression profiling for molecular distinction and characterization of laser captured primary lung cancers. *J. Transl. Med.* **6,** 69 (2008).
40. Su, A. I. *et al.* Molecular classification of human carcinomas by use of gene expression signatures. *Cancer Res.* **61,** 7388–7393 (2001).
41. Yu, K. *et al.* A precisely regulated gene expression cassette potently modulates metastasis and survival in multiple solid cancers. *PLoS Genet.* **4,** e1000129 (2008).
42. Lockwood, W. W. *et al.* DNA amplification is a ubiquitous mechanism of oncogene activation in lung and other cancers. *Oncogene* **27,** 4615–4624 (2008).
43. Shankavaram, U. T. *et al.* Transcript and protein expression profiles of the NCI-60 cancer cell panel: an integromic microarray study. *Mol. Cancer Ther.* **6,** 820–832 (2007).
44. Su, L.-J. *et al.* Selection of DDX5 as a novel internal control for Q-RT-PCR from microarray data using a block bootstrap re-sampling scheme. *BMC Genomics* **8,** 140 (2007).
45. Miyanaga, A. *et al.* Antitumor activity of histone deacetylase inhibitors in non-small cell lung cancer cells: development of a molecular predictive model. *Mol. Cancer Ther.* **7,** 1923–1930 (2008).
46. Balko, J. *et al.* Gene expression patterns that predict sensitivity to epidermal growth factor receptor tyrosine kinase inhibitors in lung cancer cell lines and human lung tumors. *BMC Genomics* **7,** 289 (2006).
47. Irizarry, R. A. *et al.* Exploration, normalization, and summaries of high density oligonucleotide array probe level data. *Biostatistics* **4,** 249–264 (2003).
48. Smyth, G. K., Michaud, J., I. & Scott, H. S. Use of within-array replicate spots for assessing differential expression in microarray experiments. *Bioinformatics* **21,** 2067–2075 (2005).
49. Hochberg, Y. & Benjamini, Y. More powerful procedures for multiple hypothesis testing. *Stat. Med.* **9,** 811–818 (1990).
50. Li, C. & Wong, W. H. Model-based analysis of oligonucleotide arrays: Expression index computation and outlier detection. *Proc. Natl Acad. Sci. USA* **98,** 31–36 (2001).
51. Curtis, S. J. *et al.* Primary tumor genotype is an important determinant in identification of lung cancer propagating cells. *Cell Stem Cell* **7,** 127–133 (2010).

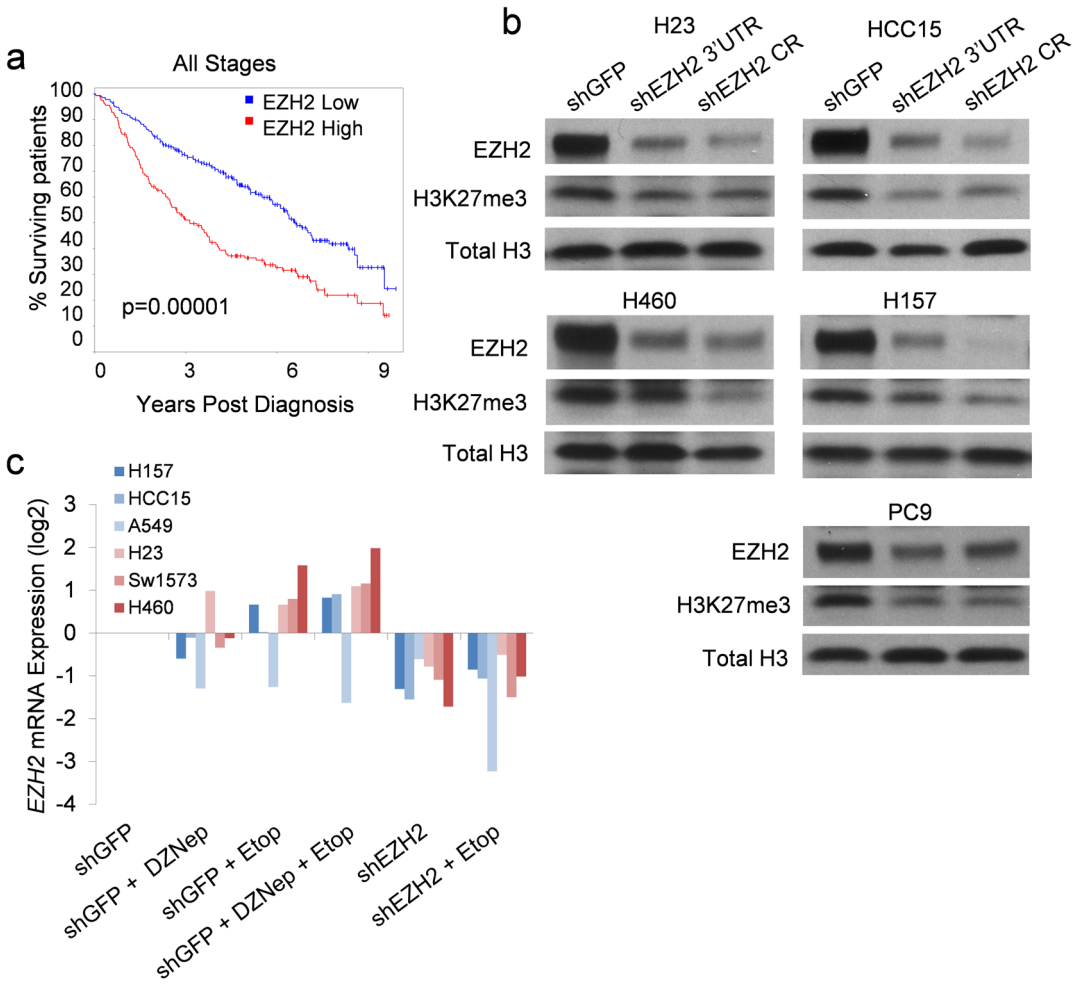

Extended Data Figure 1 | Verification of EZH2 as a potential target for NSCLC. **a**, Survival of patients with lung adenocarcinoma in the Director's Challenge data set. Samples were hierarchically clustered using the primary-tumour-generated *EZH2* co-expression signature (Supplementary Table 1) into two risk groups. The Kaplan–Meier curve for the whole data set is shown ($n = 416$, $P < 0.00001$). **b**, Western blot was performed on whole-cell extracts from indicated lines for EZH2 and its catalytic mark H3K27me3; total histone H3 is shown as loading control. CR indicates a coding region targeting hairpin. **c**, RT-qPCR for average expression of *EZH2* in the indicated cell lines after plating at equal density and treating for 4 days with indicated treatments. Each cell line is normalized to its shGFP control ($n = 2$ biological replicates).

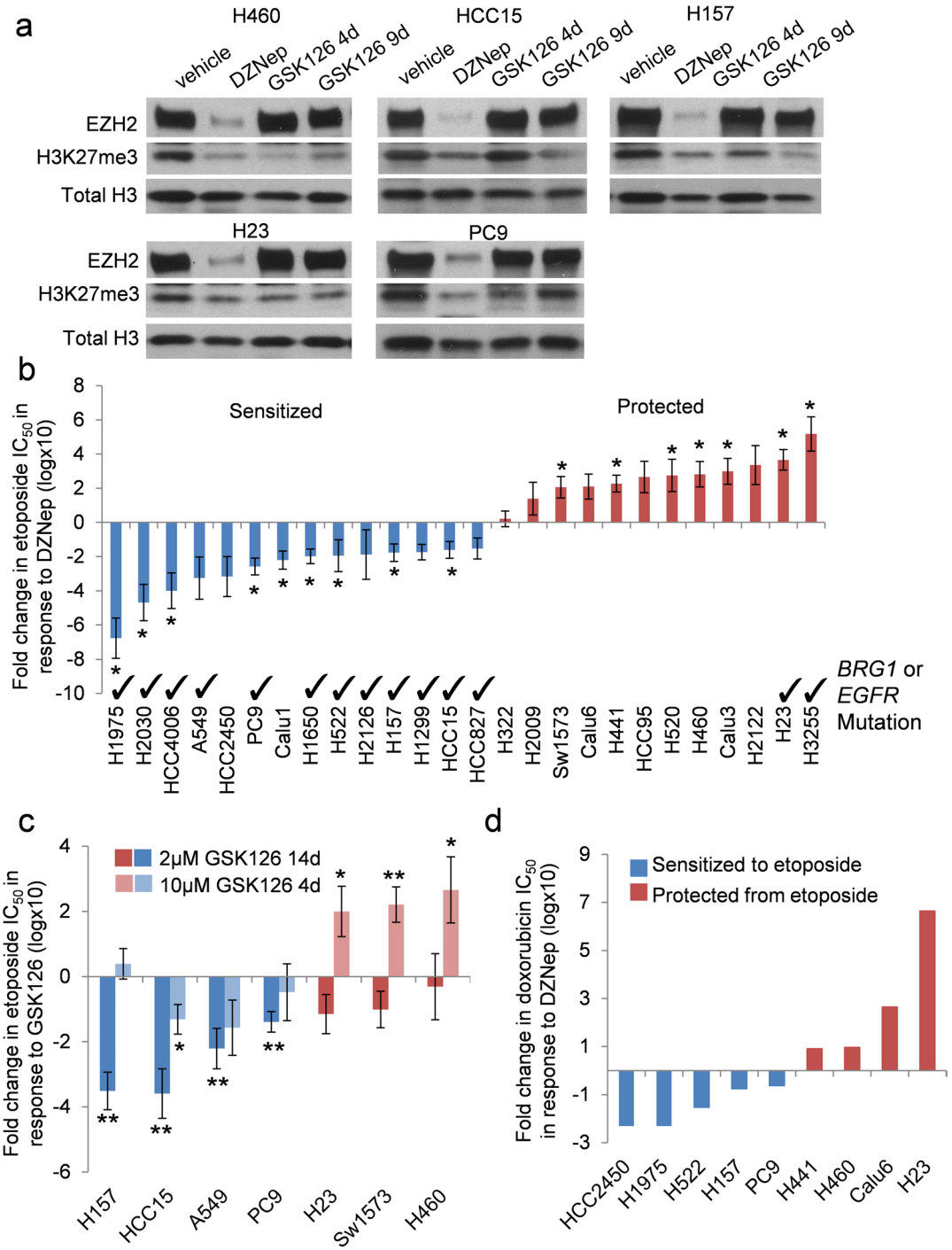

Extended Data Figure 2 | Pharmacological inhibition of EZH2 changes response of cells to TopoII inhibitors. **a**, Western blot for EZH2 and H3K27me3 was performed on whole-cell extracts after administration of 1 μM DZNep for 4 days, 10 μM GSK126 for 4 days, 2 μM GSK126 for 9 days, or vehicle. Total histone H3 is shown as a loading control. **b**, The fold change in etoposide IC_{50} ± s.e.m. in response to DZNep is plotted ($n = 3$ biological replicates for H1975, H2030, HCC4006, A549, HCC2450, Calu1, H1650, H522, H2126, H1299, HCC15, H322, H2009, HCC95, H520, H460, Calu3, H2122, H23 and H3255; $n = 4$ biological replicates for PC9, H157, HCC827, Sw1573, Calu6 and H441; $^*P < 0.02$). Cell lines with mutations in *BRG1* or *EGFR* are indicated. Note that the H23 cell line has a very late coding region mutation in BRG1 (K1533N) and is predicted to produce functional protein[22], consistent with its protected phenotype in our assays. **c**, Fold change ± s.e.m. between vehicle-treated and indicated EZH2i-treated lines for etoposide IC_{50} is plotted ($n = 3$ biological replicates; $^*P < 0.03$, $^{**}P < 0.01$). **d**, Fold change in doxorubicin IC_{50} in response to DZNep ($n = 2$ biological replicates).

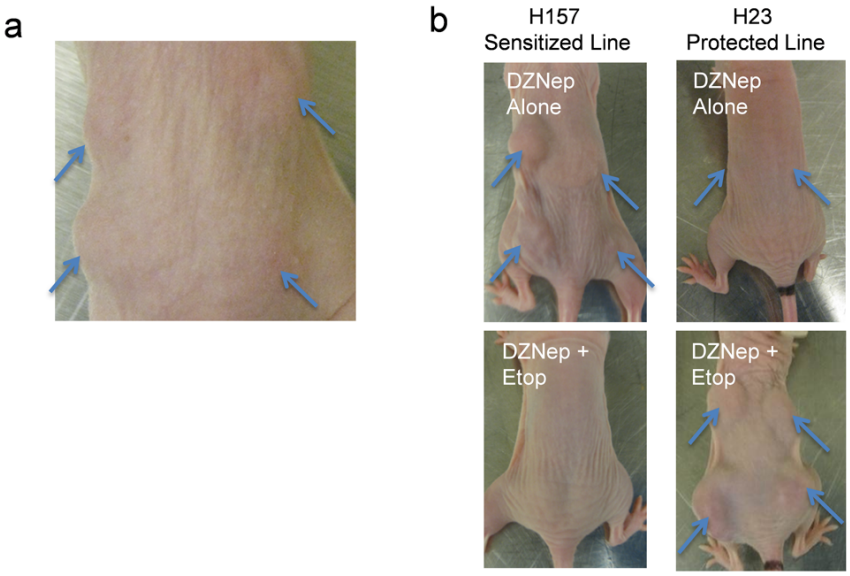

Extended Data Figure 3 | Xenograft experiments confirm sensitized and protected phenotypes. **a**, Representative image of mouse injected at four sites (arrows) with H23 tumour cells 12 days after cell injection. **b**, Representative images of mice injected at four sites with either H23 or H157 cells, and treated with indicated drugs, 35 days after cell injection. Palpable tumours that remain are indicated with arrows.

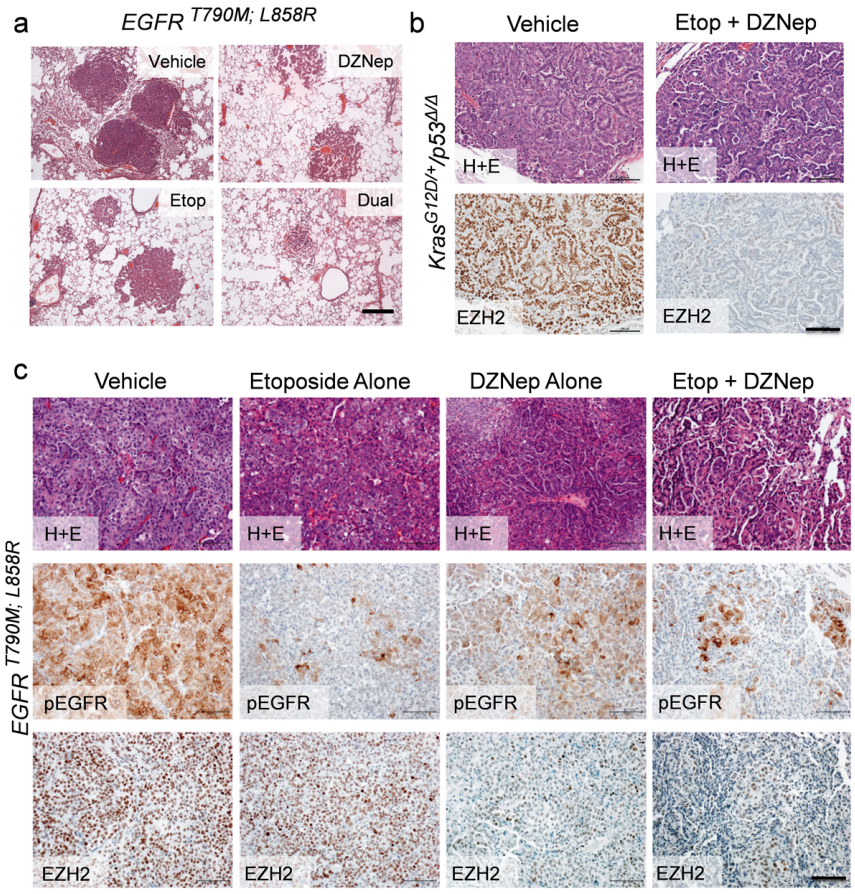

Extended Data Figure 4 | Autochthonous mouse models confirm genotype specificity of dual EZH2i and TopoIIi. **a**, Representative images of haematoxylin and eosin stained lung from $EGFR^{T790M;L858R}$ mice treated with indicated therapies for 4 weeks. Areas with tumours of similar sizes were chosen for comparison; scale bar, 200 μm. **b**, Histology from $Kras^{G12D/+}/p53^{\Delta/\Delta}$ mouse lung tumours after 1 week of indicated treatments; top image is haematoxylin and eosin, bottom image is EZH2 immunohistochemistry; scale bar, 100 μm. **c**, Histology from $EGFR^{T790M;L858R}$ mouse lung tumours after 4 weeks of indicated treatments; top image is haematoxylin and eosin, centre image is phospho-EGFR immunohistochemistry and bottom image is EZH2 immunohistochemistry; scale bar, 100 μm.

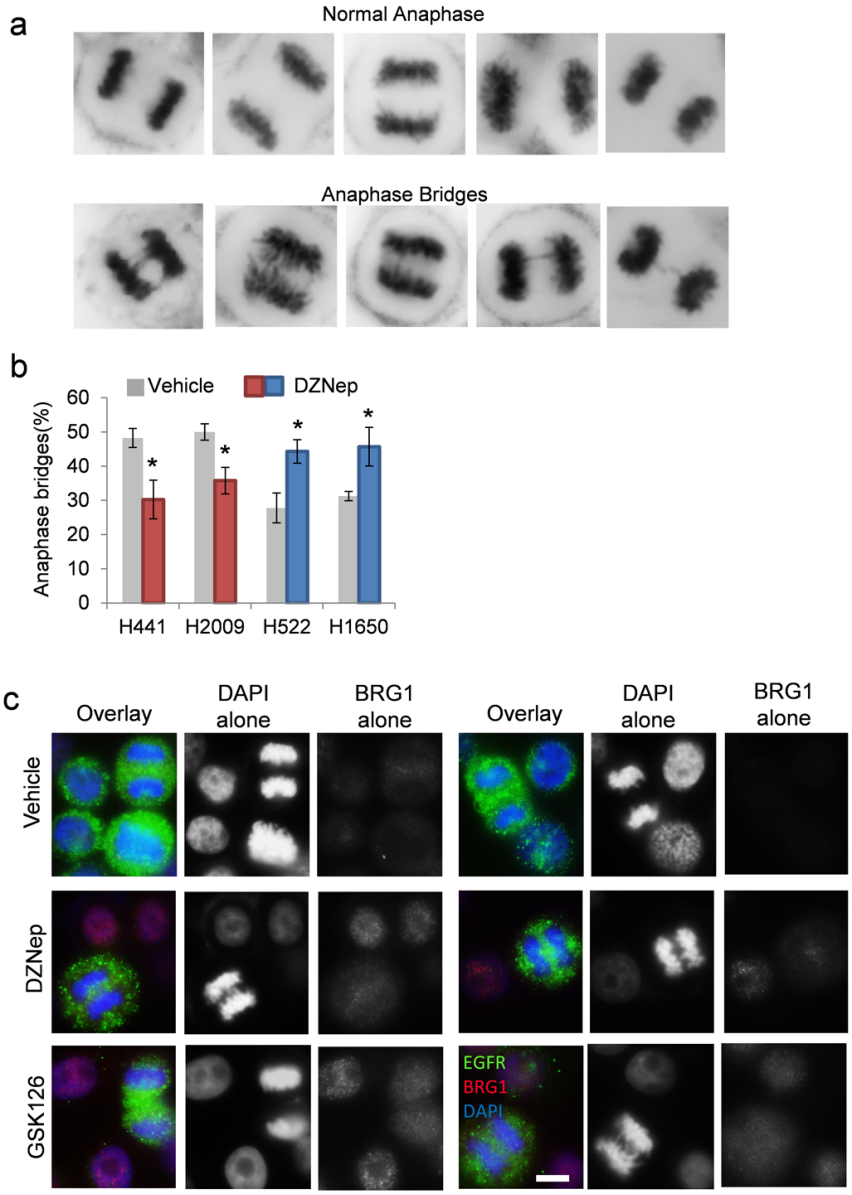

Extended Data Figure 5 | EZH2i modulates anaphase bridging differentially by genotype. **a**, Representative images of nuclei undergoing a normal anaphase and of nuclei that scored positively for the presence of anaphase bridges. **b**, Average percentage of anaphase bridging ± s.e.m. in additional *BRG1* WT H2009 and H441, *BRG1* mutant H522, and *EGFR* mutant H1650 cell lines ($n = 3$ biological replicates for all except H1650 ($n = 4$); $^*P < 0.05$). **c**, Immunofluorescence on PC9 cultures showing increase in BRG1 staining in interphase nuclei in response to EZH2i while anaphase nuclei retain strong EGFR stain, representative of three biological replicates; scale bar, 30 μm.

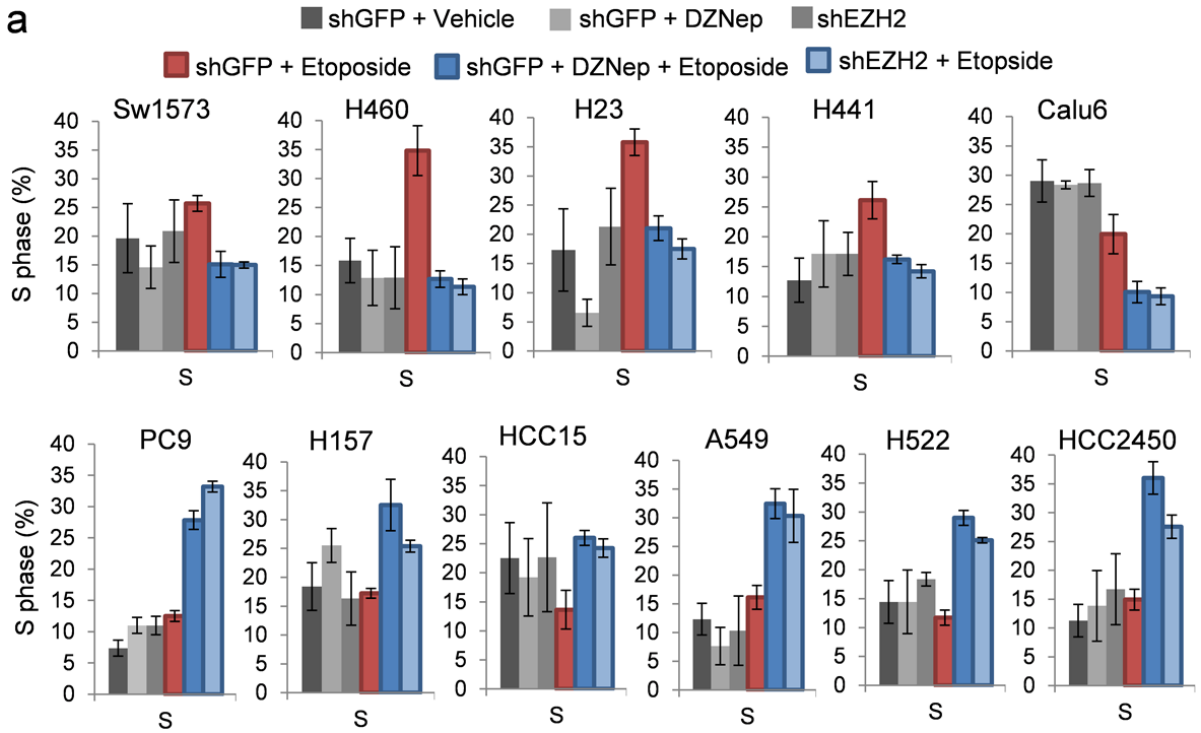

Extended Data Figure 6 | Cell cycle and apoptosis analysis of dual EZH2i- and TopoIIi-treated lines. a, 7AAD cell cycle flow cytometry on cultures corresponding to each experiment shown in Fig. 3d. The average percentage S phase ± s.e.m. of each culture is plotted ($n = 3$ biological replicates for H460, H23, Calu6, PC9, HCC15, A549 and H522; $n = 4$ biological replicates for Sw1573, H441 and H157).

a

Cell Line	*EGFR*	*BRG1*
HCC2279	E746_A750del	WT
HCC2935	E746_A750del	WT
PC14	E746_A750del	WT
A427	WT	Null
H661	WT	L1161fs*3
H1703	WT	E668_Q758del
DMS-114	WT	E1310*
RERF-LC-MS	WT	A1245fs*13
H1573	WT	E1399*
H1581	WT	E1310*
H1693	WT	L1085fs*32
H838	WT	Null
H1819	WT	L1085fs*6
H596	WT	WT
H1648	WT	WT
H1437	WT	WT
H1755	WT	WT
H2087	WT	WT
H1395	WT	WT

b

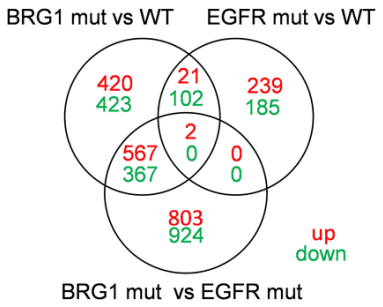

c

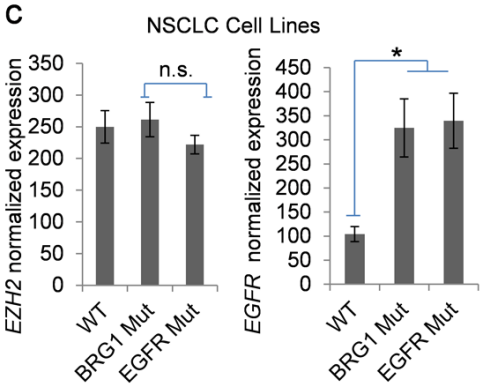

Extended Data Figure 7 | *EGFR* and *BRG1* negatively correlate in NSCLC. **a**, Additional NSCLC cell lines with known *EGFR* and *BRG1* mutations used to estimate mutually exclusivity of the two mutations. **b**, Venn diagram of differential gene expression overlap between cell lines of various genotypes. **c**, Average probe intensity ± s.e.m. of *EGFR* probe (201983_s_at) and *EZH2* probe (203358_s_at) on the U133A Affymetrix array for cell lines with various *EGFR* and *BRG1* mutational statuses ($n = 6$ per genotype, see Methods; $^*P = 0.014$).

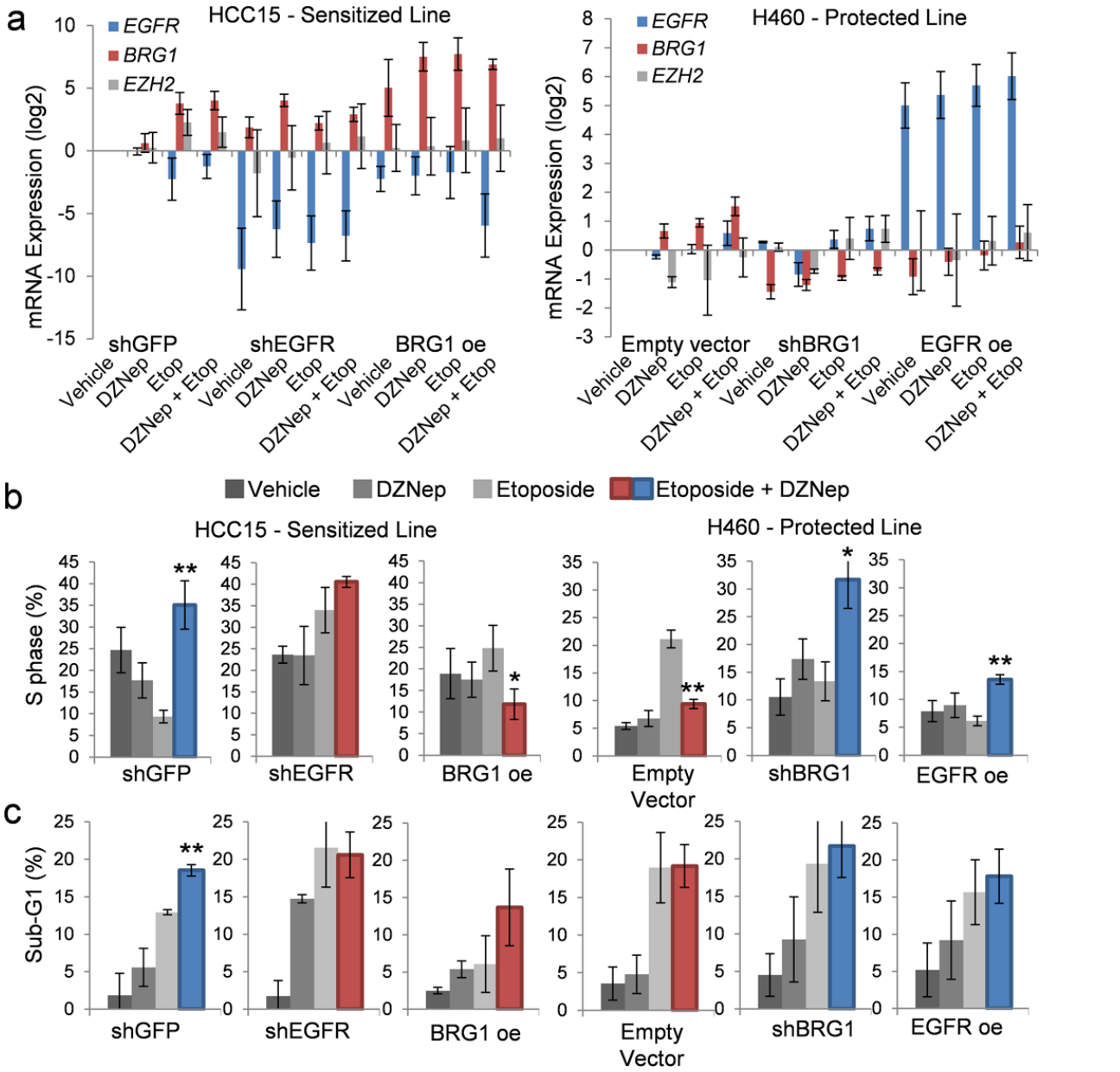

Extended Data Figure 8 | Modulation of EGFR and BRG1 influences sensitized and protected phenotypes. **a**, RT-qPCR for average expression of *BRG1*, *EGFR* and *EZH2* ± s.e.m. in the various indicated treated transduced cell lines ($n = 3$ biological replicates). **b**, For the indicated HCC15 and H460 stably transduced etoposide-treated cell lines, 7AAD flow cytometry was used to assess average changes in percentage S phase ± s.e.m. in response to DZNep ($n = 3$ biological replicates; $^{*}P = 0.02$, $^{**}P < 0.001$). **c**, Average percentage sub-G_1 fractions ± s.e.m. of the indicated 4-day cultures were assessed during 7AAD cell cycle flow cytometry analysis. Critically, for these assays, the supernatant of each culture was retained and combined with the trypsinized adherent cells to reflect the total amount of apoptosis/necrosis in each culture accurately ($n = 3$ biological replicates; $^{**}P = 0.03$).

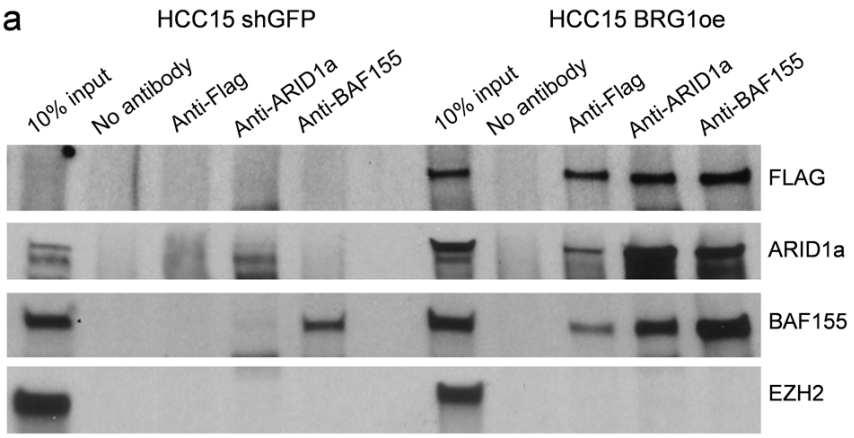

Extended Data Figure 9 | Confirmation that BRG1 re-expression leads to formation of BAF complex. **a**, Immunoprecipitation of BAF complex members from nuclear lysates of the (left) *BRG1* mutant HCC15 shGFP control cell line and (right) the HCC15 line with BRG1 re-expressed shows that exogenously expressed Flag-tagged BRG1 does result in BRG1-containing BAF complex formation. The blot is representative of three biological replicates.